Acceleration of catalysis in dihydrofolate reductase by transient, site-specific photothermal excitation

Rachel Kozlowski[a], Jing Zhao[a], and R. Brian Dyer[a,1]

[a]Department of Chemistry, Emory University, Atlanta, GA 30322

Edited by Susan Marqusee, University of California, Berkeley, CA, and approved December 1, 2020 (received for review July 10, 2020)

We have studied the role of protein dynamics in chemical catalysis in the enzyme dihydrofolate reductase (DHFR), using a pump–probe method that employs pulsed-laser photothermal heating of a gold nanoparticle (AuNP) to directly excite a local region of the protein structure and transient absorbance to probe the effect on enzyme activity. Enzyme activity is accelerated by pulsed-laser excitation when the AuNP is attached close to a network of coupled motions in DHFR (on the FG loop, containing residues 116–132, or on a nearby alpha helix). No rate acceleration is observed when the AuNP is attached away from the network (distal mutant and His-tagged mutant) with pulsed excitation, or for any attachment site with continuous wave excitation. We interpret these results within an energy landscape model in which transient, site-specific addition of energy to the enzyme speeds up the search for reactive conformations by activating motions that facilitate this search.

enzyme | dynamics | nanoparticles | photothermal

The role of protein dynamics in the mechanism of chemical catalysis by enzymes is a crucial but unresolved question (1–4). Proteins are highly dynamic molecules (5–7), but determining which protein motions might be coupled to catalysis is a difficult challenge. So far, it has not been possible to excite such motions directly while observing the effect on catalysis. Protein motions that might affect catalysis range from local fluctuations of side chains to larger-scale conformational changes (domain rotations or loop closures) and also span a wide range of timescales (8–10). These motions can be divided into two general classes: ones directly coupled to crossing the transition state and ones that facilitate the search for reactive conformations. An example of the first type would be motions that modulate the donor to acceptor distance for hydride transfer on the timescale of crossing the transition state (10^{-13} – 10^{-12} s) (6, 8, 9, 11, 12). These motions are coherently coupled to catalysis. In contrast, motions involved in the search of the energy landscape for reactive conformations are expected to be slower, on the nanosecond to microsecond timescale or longer, and they modulate the population of Michaelis state conformations rather than couple directly to catalysis (4, 13–16). Here we explore whether it is possible to directly excite this second class of motions in a model enzyme, *Escherichia coli* dihydrofolate reductase (DHFR), using laser induced heating of DHFR conjugated to a gold nanoparticle (AuNP).

AuNPs have been used previously for the photothermal heating of enzymes and peptides (17–20). A laser is used to photoexcite the surface plasmon resonance (SPR) absorbance of the AuNP (21, 22). Nonradiative relaxation through electron–electron scattering and electron–phonon coupling converts the absorbed energy into heat, resulting in a rapid temperature increase of the AuNP surface. Subsequent phonon–phonon coupling causes heat to dissipate into the surroundings (23). In this way, a protein attached to the surface of the AuNP can be rapidly and site-specifically heated by the laser pulse. This approach has been employed to study thermophilic-enzyme gold-nanorod conjugates encapsulated in calcium alginate, in which continuous light excitation (heating) of the nanorod and encapsulation from the alginate heats the enzyme and causes its activity to increase (17). The mechanism of heat transfer through small peptides attached to AuNPs was studied using heat-responsive labels on the peptide (18). Heat transfer from the AuNP to the peptide was observed to occur through the single point of attachment of the peptide, producing a time-dependent heat distribution through the peptide as the heat is transferred linearly through its backbone. The initial anisotropic heat distribution evolved to an isotropic one as the heat equilibrated linearly through the peptide structure. While these studies demonstrate that AuNPs can be used to heat an attached protein photothermally and site specifically, none have attempted to connect energy transfer from AuNPs to catalytically relevant enzyme dynamics.

We chose the enzyme DHFR as a model system because protein motions have been postulated to be coupled to its catalytic activity, but their exact role remains contentious (24–26). DHFR is a ubiquitous enzyme that catalyzes the reduction of the substrate 7,8-dihydrofolate (DHF) to 5,6,7,8-tetrahydrofolate through the oxidation of the cofactor nicotinamide adenine dinucleotide phosphate (NADPH) to $NADP^+$. The mechanism of substrate reduction involves a hydride transfer from NADPH to DHF and a concomitant proton transfer (27). Molecular-dynamics (MD) simulations have shown that there are motions across DHFR that are coupled to each other in the reactive complex but not in the product complex and these motions have been linked to catalysis by mutational studies (28–31). This network of coupled motions involves active site residue I14 and many distal residues, including A9, M42, R44, H45, T46, L54, G121, D122, and F125 (Fig. 1). These residues span the active site, which is roughly in the center of the view presented in Fig. 1.

Significance

Direct excitation of specific protein structural dynamics as a test of their role in enzyme catalysis has not yet been possible. Here we show that such motions can be excited photothermally, using a gold nanoparticle attached to a specific site on the enzyme dihydrofolate reductase (DHFR). DHFR is known to adopt multiple ground-state conformations having different kinetics of enzyme turnover. Site-specific photothermal excitation enables the enzyme to sample different reactive basins in the catalytic energy landscape and accelerates catalysis. We postulate that transient, site-specific heating excites a network of coupled motions that form a collective breathing mode of the protein structure near the active site, facilitating redistribution of the population into more reactive conformations.

Author contributions: R.K., J.Z., and R.B.D. designed research; R.K. performed research; R.K., J.Z., and R.B.D. analyzed data; and R.K. and R.B.D. wrote the paper.

The authors declare no competing interest.

This article is a PNAS Direct Submission.

[1]To whom correspondence may be addressed. Email: briandyer@emory.edu.

This article contains supporting information online at https://www.pnas.org/lookup/suppl/doi:10.1073/pnas.2014592118/-/DCSupplemental.

Published January 18, 2021.

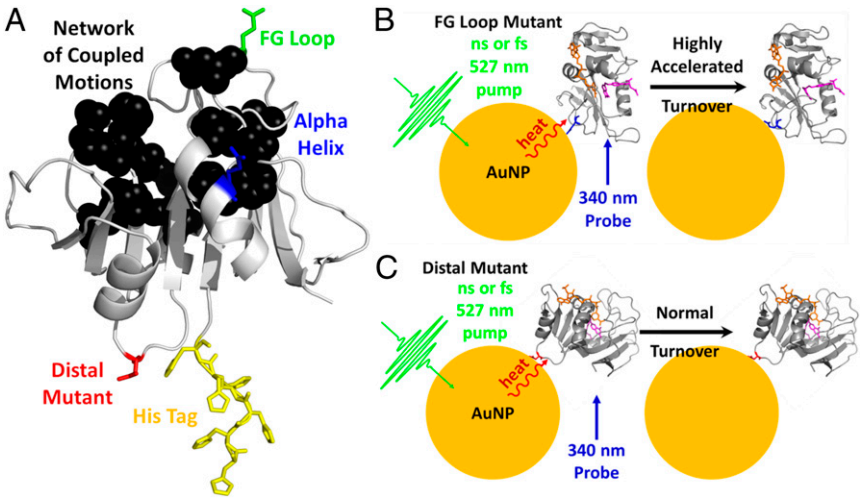

Fig. 1. Schematic of the overall experimental design. (*A*) DHFR with mutated residues labeled (Protein Data Bank, PDB: 1RX2). Green, FG loop; blue, alpha helix; red, distal mutant, and yellow, His tagged. The residues in the anticorrelated network of coupled motions are shown in black. (*B*) FG loop mutant location. E120, on the FG loop, is mutated to a cysteine for the site of AuNP attachment next to the G121 residue of the network of coupled motions. In the conjugates, there is actually a layer of protein surrounding the AuNP as described in detail elsewhere (54). (*C*) Distal mutant location. D87 is mutated to a cysteine as a control with an attachment site away from the network of coupled motions. These representations are not to scale. While one enzyme per AuNP is shown here, the experimental evidence shows that there is a monolayer of protein covering each AuNP.

MD simulations by the Brooks group showed that these residues exhibit anticorrelated motions (i.e., motions in concert but in opposite directions) in the reactive complex of DHFR (13). The anticorrelated motions of these residues can be described as a "collective breathing motion" of the protein structure spanning the active site. Mutation of any of these residues reduces the activity of the enzyme, which has been attributed to changes in the motions such that they become catalytically unfavorable. Further, L28, F31, Y100, and T113 all line the active site, and while these residues are not significantly coupled to distal residues, they affect the rate of catalysis seemingly due to the binding geometry changes from the anticorrelated motions (13).

We explored the catalytic energy landscape of DHFR by transient, site-specific heating of the protein structure. We attached AuNPs (15-nm diameter) to DHFR near and distal to the network of coupled motions (Fig. 1). Residues E120 and E101 were selected due to their proximity to the network whereas D87 and the His tag act as "control" mutants, because they are located far from the network. We studied the effect of photothermal excitation on the enzyme activity, and we also studied whether the timescale of energy input effects the outcome, using continuous and pulsed (80-fs and 20-ns) laser excitation. During catalysis, the enzyme searches the energy landscape for the most accessible reactive conformations. Our results show that this search can be accelerated by input of energy at locations next to the network of coupled motions and on the timescale for which these motions remain anticorrelated. We postulate that the search for reactive conformations is accelerated by these collective motions, which facilitate reorientation of the substrate.

Results and Discussion

Monitoring Activity of DHFR–AuNP Conjugates. The maximum catalytic rate of DHFR (v_{max}) was measured for the DHFR–AuNP conjugates at saturating substrate concentrations using the 340-nm NADPH absorbance to follow the kinetics and k_{cat}, was determined by dividing v_{max} by the enzyme concentration (Table 1). Saturation conditions were achieved with 50 μM of substrate, an order of magnitude larger than the K_m of DHFR of 4.8 μM (27). In general, we observe decreased enzyme activity in the conjugates, a common occurrence for enzymes attached to surfaces that has been attributed to a variety of factors, including increased stability and decreased flexibility of the structure (32–35). There are also differences in activity that depend on the mode of conjugation to the surface. The distal mutant conjugate retains slightly more activity than the others (Table 1 and *SI Appendix*, Fig. S2*D*), likely because its cofactor and substrate binding sites are more solvent exposed. The FG loop and alpha helix mutant conjugates have less favorable orientations of the enzyme on the AuNP surface that may partially block the cofactor binding site, or they may hinder the loop motions required for catalysis, resulting in lower activity. The His-tagged conjugate also exhibits lower activity despite a favorable orientation on the AuNP surface, possibly due to its higher surface coverage (*SI Appendix*), which may sterically hinder access of the substrate or cofactor.

Laser Heating of the DHFR–AuNP Conjugates. We measured the effect of laser heating on enzyme catalysis with pump–probe experiments in which a pump laser excited the AuNP SPR band and heated the DHFR–AuNP conjugates and the enzyme kinetics were probed using the 340-nm NADPH cofactor absorbance. To observe an effect of laser heating on the DHFR kinetics, we hypothesize that the heat input must be localized to the network of coupled motions and it must be on a timescale that is on the order of the energy redistribution time or faster and can therefore preferentially excite the motions of the protein that are coupled to catalysis. The initial energy input was localized by attaching the AuNP to a specific site on the protein surface, either adjacent to (FG loop and alpha helix) or remote from (distal network and His tagged) the network of coupled motions. Furthermore, the initial heating of the protein structure is localized to the point of attachment and the nearby structure. The point of attachment is not at the active site, so any heating of the active site is indirect, either through the network of coupled motions or by diffusive heat flow. The pump and probe beams were overlapped in the sample such that the probe only measured the activity of the AuNP–DHFR conjugates being excited (locally heated) by the pump beam (*SI Appendix*, Fig. S4). The heating is transient and localized to the

Table 1. k_{cat} of DHFR–AuNP conjugates in steady-state turnover, with and without laser illumination

	k_{cat} (s^{-1})				
Sample type	Free protein	-AuNP,* No laser	-AuNP,* CW	-AuNP,* ns	-AuNP,* fs
FG loop	27.2 ± 0.3[†]	0.645 ± 0.048	100 mW: 0.592 ± 0.028 250 mW: 0.653 ± 0.053	50 mW: 0.568 ± 0.030 100 mW: 1.143 ± 0.032 200 mW: 1.105 ± 0.048	5 mW: 0.694 ± 0.031 20 mW: 0.690 ± 0.035 40 mW: 1.270 ± 0.032
Alpha helix	30.0 ± 0.3	0.769 ± 0.047	100 mW: 0.781 ± 0.023 250 mW: 0.837 ± 0.088	50 mW: 0.750 ± 0.045 100 mW: 1.200 ± 0.048 200 mW: 1.221 ± 0.045	5 mW: 0.722 ± 0.055 20 mW: 0.745 ± 0.102 40 mW: 1.302 ± 0.088
His tagged	29.6 ± 0.4	0.759 ± 0.035	100 mW: 0.742 ± 0.071 250 mW: 0.756 ± 0.041	50 mW: 0.781 ± 0.070 100 mW: 0.792 ± 0.062 200 mW: 0.836 ± 0.026	5 mW: 0.758 ± 0.038 20 mW: 0.769 ± 0.028 40 mW: 0.798 ± 0.037
Distal mutant	30.1 ± 0.4	1.073 ± 0.083	100 mW: 1.004 ± 0.062 250 mW: 1.079 ± 0.053	50 mW: 1.176 ± 0.088 100 mW: 0.981 ± 0.079 200 mW: 1.032 ± 0.059	5 mW: 1.117 ± 0.057 20 mW: 1.175 ± 0.020 40 mW: 1.199 ± 0.010

*Conjugates with 15-nm AuNPs.
[†]Uncertainties represent SDs of at least three trials.

conjugate, such that there is no detectable rise in temperature of the enzyme solution over the course of the kinetics measurement. We also explored the effect of the timescale of heating, using pulsed (80 fs or 20 ns) or continuous wave excitation. The short time limit for heat input is set by the rate of conversion of the absorbed light energy to heat in the AuNP (~1 ps) which can be achieved using ultrafast laser excitation, whereas continuous wave laser excitation allows us to heat the enzyme on a timescale that is slow compared to the energy redistribution time.

Pulsed-Laser Heating. Transient heating of the FG loop and alpha helix conjugates with 20-ns pulses and an average pump power of 50 mW produced no detectable effect on k_{cat} (Fig. 2 *A* and *B*), but at higher pump powers a marked acceleration in rate was observed. The FG loop conjugate showed a 75% increase in activity, while the alpha helix conjugate showed a 56% increase in activity. This rate acceleration saturates since no further change was observed when the pump power was increased from 100 to 200 mW. When the average power was increased above 200 mW, the noise drastically increased, likely due to cavitation

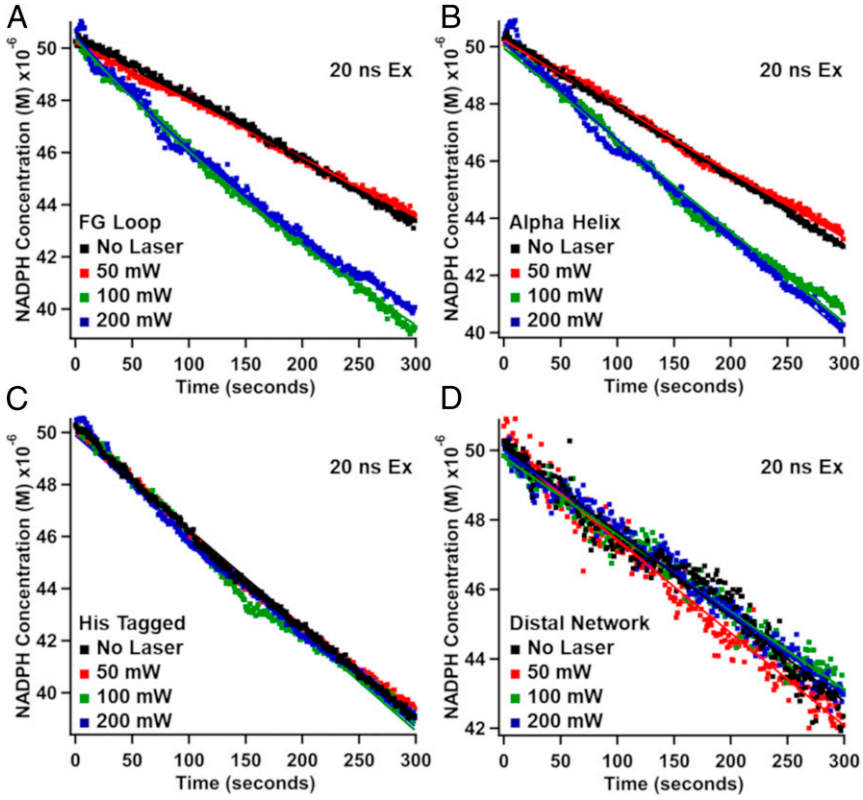

Fig. 2. Rate dependence on nanosecond pulsed-laser excitation. (*A*) FG loop–15-nm AuNP conjugates. Laser power of 100 mW or greater shows a 75% increase in activity. (*B*) Alpha helix–15-nm AuNP conjugates. Laser power of 100 mW or greater shows a 56% increase in activity. (*C*) His tagged–15-nm AuNP conjugates. (*D*) Distal mutant–15-nm AuNP conjugates: No increase in activity with any amount of nanosecond laser excitation. Reaction conditions for all assays: 10–30 nM enzyme, 50 μM substrate, 50 μM cofactor at 37 °C for 5 min.

caused by the high peak power of individual pulses (36). Consequently, we kept the average power below 200 mW to avoid this noise problem. The distal mutant and His-tagged conjugates showed a different result altogether. No increase in activity with any amount of 20-ns pulsed laser power was observed for either of these two conjugates (Fig. 2 *C* and *D*). These mutants are each attached to the AuNP away from the network of coupled motions in DHFR, so the addition of heat in this case does not heat the network directly. The distal mutant and His-tagged mutant are also experimental controls for questions regarding the bulk heating of solution. If substantial bulk heating of the surrounding solution were the underlying cause of the rate acceleration, an increase in activity would also be observed for these two conjugates. Since we observe no such acceleration, this supports the conclusion that the initial heating of the protein is localized at the point of attachment of the AuNP; on a longer timescale the heat is redistributed throughout the protein structure and dissipates to the surroundings, but the net change in temperature is insufficient to affect catalysis (see COMSOL simulations and Arrhenius analysis).

With the three Cys mutant–AuNP conjugates, we expect the net heat transfer into the protein to be the same regardless of the attachment point, since it occurs through the same linkage in each case. Therefore, the observed differences in catalytic activity depend on where the heat is input with respect to the network of coupled motions. It is clear that a maximum effect on the catalysis is achieved when the heat is input more directly into the network of coupled motions in DHFR.

Similar results were observed for excitation of the AuNP–DHFR conjugates with 80-fs laser pulses (Fig. 3). For the FG loop and alpha helix conjugates, there is an increase in activity with sufficient power of the 80-fs pulsed laser (Fig. 3). With 40-mW pump power, the FG loop conjugates show a 95% increase in activity, and the alpha helix conjugates show a 75% increase in activity. The effects of pulsed heating are greater with 80-fs compared to 20-ns pulses, suggesting that the acceleration of the search of the energy landscape is more efficient with the input of heat on a faster timescale. As with the nanosecond pulsed excitation, the distal mutant and His-tagged conjugates do not show increased turnover with any amount of laser excitation power (Fig. 3 *C* and *D*). This is further evidence that addition of heat on the network of coupled motions in DHFR is obligatory for photothermally induced rate acceleration, likely due to the facilitated search for reactive conformations.

Continuous Wave Laser Heating. As a control, a continuous wave (CW) laser was used as a pump excitation source, but with the same average power as the pulsed-laser excitation, such that the average heating of the sample was the same over the course of the enzyme kinetics measurement. There was no difference in the observed turnover rate induced by heating any of the DHFR–AuNP conjugates with any amount of CW excitation (Fig. 4). All turnover rates are expressed quantitatively in Table 1. Although the same total energy is added to the system in both the pulsed and CW heating experiments, in the case of CW excitation the energy input is much slower than the redistribution time. Since the net temperature change is negligible once the heat is distributed throughout the protein, the result is no change in the enzyme activity.

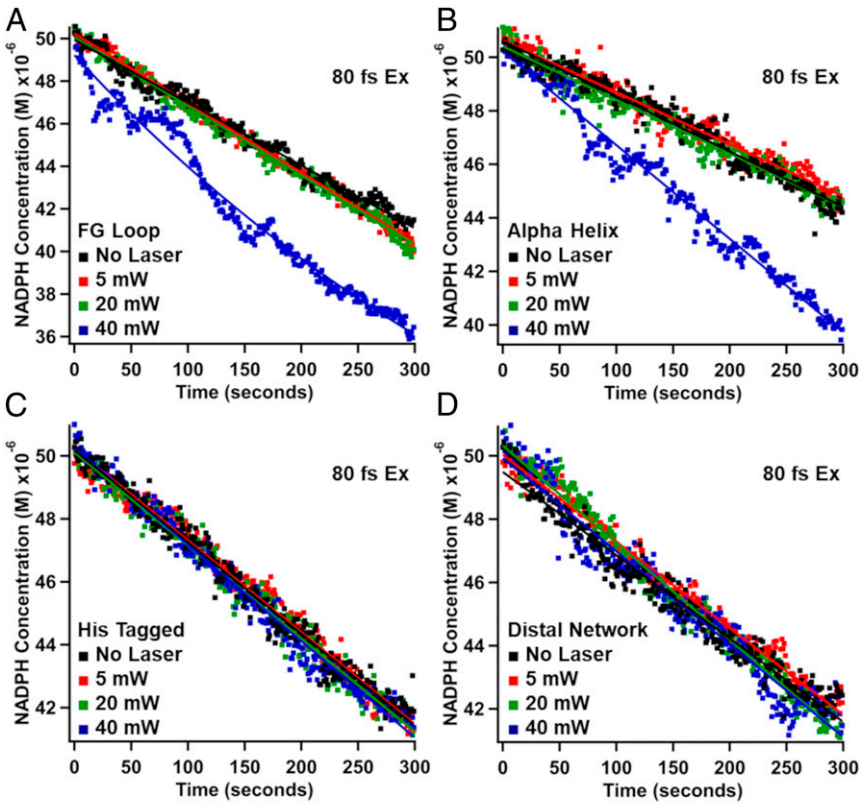

Fig. 3. Rate dependence on femtosecond pulsed laser excitation. (*A*) FG loop–15-nm AuNP conjugates. Laser power of 40 mW shows a 95% increase in activity. (*B*) Alpha helix–15-nm AuNP conjugates. Laser power of 40 mW shows a 75% increase in activity. (*C*) His tagged–15-nm AuNP conjugates. (*D*) Distal mutant–15-nm AuNP conjugates: No increase in activity with any amount of femtosecond laser excitation. Reaction conditions for all assays: 10–30 nM enzyme, 50 μM substrate, 50 μM cofactor at 37 °C for 5 min.

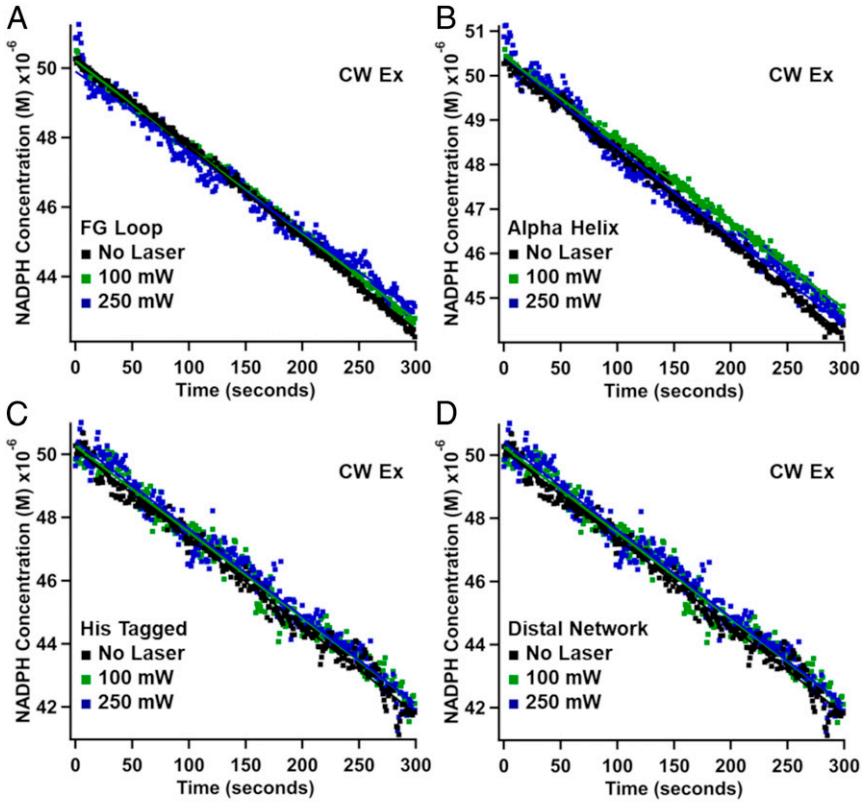

Fig. 4. Rate dependence on CW laser excitation. (*A*) FG loop–15-nm AuNP conjugates. (*B*) Alpha helix–15-nm AuNP conjugates. (*C*) His tagged–15-nm AuNP conjugates. (*D*) Distal mutant–15-nm AuNP conjugates. None of the conjugates show any increase in activity with any power of CW laser excitation. Reaction conditions for all assays: 10–30 nM enzyme, 50 μM substrate, 50 μM cofactor at 37 °C for 5 min.

Finite-Element Simulation of Heat-Transfer Dynamics. We used COMSOL Multiphysics package to perform a finite-element simulation of the heat-transfer dynamics and temperature gradient in the AuNP–DHFR bioconjugate during the pulsed-laser excitation and subsequent thermal relaxation (Fig. 5). These simulations were performed using three-dimensional heat-transfer equations to calculate the heat dissipation and the temperature gradient in the surrounding environment (details of the simulation are provided in *SI Appendix*). Initially, there is a large increase in temperature of the AuNP core and AuNP surface, which is very short-lived (Fig. 5 and *SI Appendix*, Figs. S6 *C* and *D* and S7*A*). This heat is transferred to the protein locally, at the point of attachment, heating this local region of the enzyme. At longer times the energy is dissipated over a larger volume, including the full protein structure and the surrounding solution, such that the net change in temperature is quite small

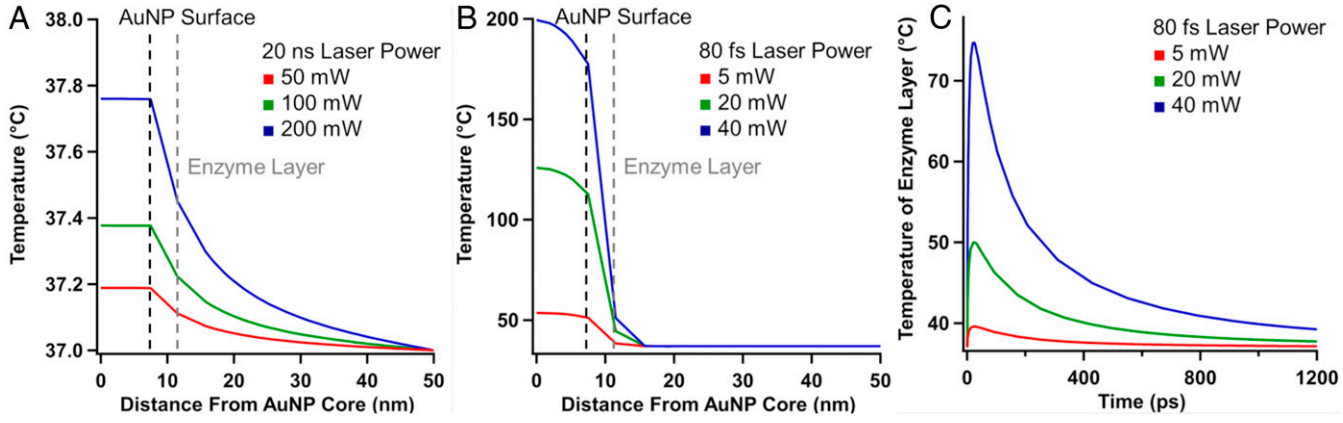

Fig. 5. COMSOL finite-element analysis of pulsed-laser excitation of AuNP–DHFR bioconjugates. (*A*) The initial (20-ns) temperature change of the AuNP and enzyme layer for the 20-ns excitation for 50, 100, and 200 mW. (*B*) The initial (80-fs) temperature change for the 80-fs excitation plotted versus the distance from the center of the AuNP for 5-, 20-, and 40-mW laser powers. For all three powers and both the nanosecond and femtosecond excitations, the temperature profile is uniform throughout the AuNP itself; then, once on the AuNP surface, there is a nonlinear decrease in temperature until equilibrated with the bulk solution temperature. (*C*) Time dependence of the temperature increase at the enzyme:bulk solvent interface after 80-fs laser excitation; the large initial increase is completely dissipated by 2 ns.

(Fig. 5), especially for nanosecond excitation. Therefore, a critical feature of the pulsed-laser excitation is the substantial transient heating that occurs in a small region of the protein structure. The initial rise and decay of the transient heating span the timescale determined by MD simulations for the correlated motions in DHFR.

With the 20-ns excitation, the temperature on the immediate surface of the AuNP increases by very little, only 15 °C above room temperature (Fig. 5*A*). Further, the heat dissipation on longer timescales (50 ns) shows complete equilibration with the surroundings. This makes physical sense because the laser pulses are 20 ns, the dissipation of heat from the AuNP occurs on the order of hundreds of picoseconds, and the repetition rate of the pulses is 5 kHz (one pulse every 200 μs). All of the heat from a single pulse has dissipated well before the next pulse arrives so there is no accumulation of heat between pulses. However, experimentally, we observe an acceleration in turnover with this nanosecond excitation. Apparently, an elevation of 15 °C above room temperature is enough to push the enzyme out of trapped, unreactive states.

There is a much higher initial temperature jump with the 80-fs excitation, as expected (Fig. 5*B*). With 40 mW of laser power, the temperature at the AuNP core is roughly 200 °C. The heat dissipates as it transfers through the surroundings, reaching the bulk solution temperature of 37 °C about 15 nm away from the AuNP core. All of the heat in the 4-nm enzyme layer dissipates within 2 ns after the initial femtosecond pulse (Fig. 5*C*). The laser pulse duration is 80 fs, and the repetition rate is 1 kHz, or one pulse every millisecond. While the peak pulse power is very high in an 80-fs pulse, the 1-kHz pulse rate allows for complete cooling before the next pulse arrives, meaning that there is no cumulative heating over the course of the experiment.

Temperature-Dependent Kinetics of the DHF–AuNP Conjugates. We measured the temperature-dependent kinetics of DHFR and performed an Arrhenius analysis to determine the expected change in rate for the bulk temperature change predicted by the COMSOL simulations. The temperature dependence of DHFR kinetics on the bulk temperature of the solution is typical of an activated process. This Arrhenius relationship was investigated with each of the free-protein mutants and their respective conjugates (*SI Appendix*, Figs. S8–S10). The activation energies of the conjugates are all similar to each other, and they are also similar to the respective free protein E_a (*SI Appendix*, Figs. S9 and S10), indicating that there is no substantial difference in bulk heating effects between any of the mutants or their respective conjugates. The Arrhenius analysis predicts that that an increase in bulk temperature of 8.8 °C would be required to produce the 95% rate enhancement observed for the FG loop conjugate with 80-fs laser excitation. However, the COMSOL simulations indicate that the heat has mostly dissipated to the surroundings within 2 ns, such that the net increase in temperature is negligible on the timescale of enzyme turnover. Therefore, the bulk heating produced by the laser excitation is much too small to generate the observed turnover acceleration. Further, transmission electron microscopy (TEM) studies show that the increase in temperature with 80-fs laser excitation does not seem to deform the AuNPs or unbind enzyme (*SI Appendix*, Figs. S11 and S12).

Conclusions

We explored the effect of transient and site-specific heating of the protein structure on the rate of DHFR catalysis. Photothermal heating of a local region of the protein structure was accomplished using a covalently attached AuNP, which converts the energy of the absorbed photons to heat on an ultrafast timescale and transfers that energy to the attached enzyme site-specifically. With pulsed-laser excitation, it is possible to excite a single AuNP with hundreds of photons per pulse (227 kJ per mole of 527-nm photons) and to transfer some of this energy to the protein much faster than the timescale of dissipation to the surrounding solution. The rate of DHFR turnover was accelerated by photothermal heating with 20-ns or 80-fs laser pulses for the FG loop and alpha helix–AuNP conjugates.

We interpret the observed rate acceleration in terms of an energy landscape model for catalysis in which the local input of heat speeds up the search for reactive conformations of the enzyme on a rough protein energy landscape (9, 37, 38). If the catalytic landscape is rough, it is likely to have multiple transition barriers with a range of heights (4, 9), and some of the enzyme population could become trapped in local minima that have high barriers to reaction. Support for this view comes from a recent single-molecule nanopore study of DHFR which observed four different ground-state conformers of the enzyme, where each conformer is postulated to have a different affinity for different states in the catalytic cycle (39). These single-molecule experiments are consistent with ensemble results, which show the enzyme cycles through multiple structures involving loop and domain motions that correspond to different catalytic intermediates (40). These conformers represent separate minima in the DHFR multidimensional energy landscape, with barriers between them. Interconversion among these ground-state conformers is likely slow under equilibrium conditions; for example, the two forms of DHFR with different affinities for the inhibitor methotrexate interconvert with a rate of 0.035 s^{-1} (41). It is also possible that there are multiple conformers within the Michaelis complex with different reactivities, due to varying orientations of the substrate or nicotinamide hydride donor. It has been shown that different substrate analogs, including folate and methotrexate, bind with different geometries in the active site (40). We conclude that local input of heat into the protein structure speeds up the interconversion among multiple DHFR conformations and helps to transfer population to more reactive basins on the landscape, from which the transition barrier is lower. In this energy landscape picture, the site-specific addition of energy to the enzyme speeds up the search for reactive conformations by activating motions that facilitate this search.

The question remains, how does the protein achieve efficient transfer of the photothermal energy to the active site to enable this conformational search? Finite-element simulations of the heat-transfer dynamics show a rapid exponential decay of the temperature with distance from the AuNP surface. These simulations are in agreement with experimental observation of energy transport and dissipation in protein structures on the hundreds of picoseconds timescale (42–45). If the photothermal energy is rapidly redistributed throughout the protein structure it is likely to have little effect on the population of active site conformations. We postulate that in addition to this diffusive energy transport, some of the energy directly excites the network of coupled motions and this collective "breathing motion" of the protein enables a more efficient search of reactive conformations. There are multiple lines of evidence to support this model. First, the energy input must be localized on or near the protein structure containing the network of coupled motions, since we do not observe acceleration of catalysis when energy is input to other parts of the protein structure. Second, the acceleration of catalysis requires input of a threshold level of energy and it saturates at higher energy input. It is difficult to rationalize these observations in terms of local heating through an equilibrium diffusion process, which should result in a Boltzmann distribution of populations that continuously shifts with increasing energy input and thus temperature. In contrast, a nonequilibrium process such as directed energy transfer into a collective motion of the protein requires a threshold energy to activate the motion and therefore should exhibit a discontinuous effect on catalysis. This effect would be expected to saturate once the population of

inactive conformation is depleted. Third, the energy must be input on the appropriate timescale, such that the coupling outcompetes the energy dissipation. MD simulations of DHFR have shown that the anticorrelation of the motions of the network occurs on a timescale of 1–10 ns (13). Efficient coupling to this collective motion requires energy input on a similar (nanosecond) timescale. Although excitation with 80-fs pulses produces significantly higher increase in temperature than 20-ns pulses, it does not produce a proportionate increase in catalytic rate, consistent with the excitation of a collective motion on the nanosecond timescale. Finally, the collective breathing motion spans the active site and modulates its structure, which may allow the substrate complex to access different conformations, providing a molecular mechanism for sampling the energy landscape. This model also accounts for the large difference in timescale between the collective protein motion (10^{-10} – 10^{-8} s) and the timescale of enzyme turnover (10^{-3} s). Local heating of the enzyme and activation of the coupled network allows redistribution of the population on the fast timescale and this new population distribution then allows accelerated turnover on the slower timescale, since conformational redistribution is slow at room temperature (41).

In summary, these results demonstrate the important role of the search for reactive conformations in DHFR catalysis by photothermal excitation and redistribution of population on the energy landscape of catalysis, to produce an acceleration in enzyme turnover. This approach can be broadly extended to other enzyme systems, especially those which have known networks of motions, such as Cyclophilin A and Triose Phosphate Isomerase (46–48). The study of heat flow through enzymes is a new approach to the characterization enzyme dynamics, providing experimental evidence on the energy landscape of enzymes and energy transfer through networks of motions in enzymes, thus furthering our knowledge of the role of motions in enzyme catalysis.

Materials and Methods

Materials. All chemicals were used as purchased from Sigma-Aldrich unless otherwise indicated. DHF was synthesized using the dithionite reduction method (49), lyophilized, and stored away from light at −20 °C with desiccant. AuNPs were synthesized using the citrate reduction method and stored away from light at 4 °C (50).

Enzyme Activity Assays. Activity assays were run by monitoring the decrease in 340-nm absorbance on an Ocean Optics QE65000 spectrometer with a xenon lamp source, following the oxidation of NADPH to $NADP^+$. To run the assays, 50 mM sodium phosphate pH 7 buffer, NADPH (50 μM), and DHFR (10–30 nM) were added into a cuvette and allowed to equilibrate at 37 °C in an Ocean Optics QPOD temperature-controlled cuvette stage for 5 min. DHF (50 μM) was added to initiate the reaction, and the 340-nm absorbance was measured over 5 min. All reactions were run in at least triplicate. Enzyme turnover was calculated by method of initial rates, which was either linear or exponential depending on the sample. For the exponential fits, preexponential (A) and τ parameters from an exponential fit were used with the integrated extinction coefficient for NADPH (11,800 $M^{-1}{\cdot}cm^{-1}$) to determine the initial rate of the reaction. The linear fits were used with the integrated extinction coefficient to determine the initial rate. The concentration of protein was used with the initial rate to determine enzyme turnover (in s^{-1}).

Laser-Heating Assays. The assays were performed as described in *Enzyme Activity Assays*, with the addition of either the CW, 20-ns pulsed, or 80-fs pulsed lasers. The CW laser was a Verdi Coherent 531-nm, 5-W CW pump laser. The nanosecond laser was a CrystaLaser diode pumped Q-switched 527-nm laser with 20-ns pulses set to 5.0-kHz repetition rate. The femtosecond pulses were generated by a Coherent ultrafast laser system described elsewhere (51–53) to produce 530-nm light in 80-fs pulses with a 1.0-kHz repetition rate. In all cases, the laser was aligned perpendicularly to the xenon lamp source in the cuvette stage (*SI Appendix*, Fig. S4). The green lasers do not interfere with the probing of the sample, as the beams cross the sample perpendicular to the probe beam and are terminated into a beam dump or power meter for laser-power determination. The power of the laser was attenuated with a continuous variable neutral density filter and monitored with a power meter after interaction with the sample. The power absorbed by the sample is roughly half of the initial power; for example, for a typical 40-mW power trial, the power measured through the sample was 20 mW. The sample was continuously illuminated with the laser throughout the entire 5-min duration of the activity measurements. The laser was aligned by inserting a fiber-optic cable into the holder on the receiving end of the laser in cuvette stage (in place of the beam dump) and placing two pinholes into the sample holder. This fiber-optic cable was attached to the spectrometer. The mirrors directing the laser into the cuvette stage were adjusted to maximize the laser intensity through the pinholes and onto the centered fiber, which maximizes alignment with the fiber-optic coupled xenon lamp source in the perpendicular holders on the cuvette holder.

Before the assay, the sample was allowed to equilibrate at 37 °C with the laser blocked. DHF was added to initiate the reaction, and the laser block was immediately removed upon start of data collection. Laser power was attenuated with a variable neutral density filter, from 50 to 200 mW for nanosecond experiments and from 5 to 40 mW for femtosecond experiments. The pump laser diameter was 2 mm, fully spanning the open length of the microvolume Starna Cells fluorescence cuvette, allowing all of the sample being probed to be excited with the pump beam. The probe beam diameter was 1 mm, allowing only the pumped sample to be probed.

Arrhenius Kinetics. The activity assays were run as described in *Enzyme Activity Assay*. The assays were run at six different temperatures: 22, 27, 32, 37, 42, and 47 °C. The raw data were fit to linear or exponential fits (*SI Appendix*, Fig. S8). The natural log of the rates is plotted on the *y* axis of the Arrhenius plots, and the respective inverse temperatures are on the *x* axis (*SI Appendix*, Figs. S9 and S10). The slope of the line was used to determine the activation energy, E_a, as it represents $-E_a/R$, where R is the gas constant 8.314 J/K·mol. The rates and temperatures were plotted as ln(rate) vs. inverse temperature, such as the Arrhenius equation: $\ln(\text{rate}) = (-E_a/R)(1/T)$.

Data Availability. All study data are included in the article and *SI Appendix*.

ACKNOWLEDGMENTS. This study was supported in part by the Emory Integrated Genomics Core, which is subsidized by the Emory University School of Medicine and is one of the Emory Integrated Core Facilities. Additional support was provided by the National Center for Advancing Translational Sciences of the NIH under Award UL1TR000454. This work was supported by NIH Grants GM068036 and GM53640 (to R.B.D.). The content is solely the responsibility of the authors and does not necessarily reflect the official views of the NIH.

1. S. Hammes-Schiffer, S. J. Benkovic, Relating protein motion to catalysis. *Annu. Rev. Biochem.* **75**, 519–541 (2006).
2. M. H. M. Olsson, W. W. Parson, A. Warshel, Dynamical contributions to enzyme catalysis: Critical tests of a popular hypothesis. *Chem. Rev.* **106**, 1737–1756 (2006).
3. D. R. Glowacki, J. N. Harvey, A. J. Mulholland, Taking Ockham's razor to enzyme dynamics and catalysis. *Nat. Chem.* **4**, 169–176 (2012).
4. R. Callender, R. B. Dyer, The dynamical nature of enzymatic catalysis. *Acc. Chem. Res.* **48**, 407–413 (2015).
5. L. Y. P. Luk, E. J. Loveridge, R. K. Allemann, Protein motions and dynamic effects in enzyme catalysis. *Phys. Chem. Chem. Phys.* **17**, 30817–30827 (2015).
6. P. Singh, T. Abeysinghe, A. Kohen, Linking protein motion to enzyme catalysis. *Molecules* **20**, 1192–1209 (2015).
7. J. P. Richard, Protein flexibility and stiffness enable efficient enzymatic catalysis. *J. Am. Chem. Soc.* **141**, 3320–3331 (2019).
8. J. P. Klinman, A. Kohen, Hydrogen tunneling links protein dynamics to enzyme catalysis. *Annu. Rev. Biochem.* **82**, 471–496 (2013).
9. S. J. Benkovic, G. G. Hammes, S. Hammes-Schiffer, Free-energy landscape of enzyme catalysis. *Biochemistry* **47**, 3317–3321 (2008).
10. R. K. Allemann, R. M. Evans, E. J. Loveridge, Probing coupled motions in enzymatic hydrogen tunnelling reactions. *Biochem. Soc. Trans.* **37**, 349–353 (2009).
11. J. R. E. T. Pineda, R. Callender, S. D. Schwartz, Ligand binding and protein dynamics in lactate dehydrogenase. *Biophys. J.* **93**, 1474–1483 (2007).
12. J. E. Basner, S. D. Schwartz, Donor–acceptor distance and protein promoting vibration coupling to hydride transfer: A possible mechanism for kinetic control in isozymes of human lactate dehydrogenase. *J. Phys. Chem. B* **108**, 444–451 (2004).
13. J. L. Radkiewicz, C. L. Brooks, III, Protein dynamics in enzymatic catalysis: Exploration of dihydrofolate reductase. *J. Am. Chem. Soc.* **122**, 225–231 (2000).
14. Z. D. Nagel, J. P. Klinman, Tunneling and dynamics in enzymatic hydride transfer. *Chem. Rev.* **106**, 3095–3118 (2006).

15. L. Wang, N. M. Goodey, S. J. Benkovic, A. Kohen, The role of enzyme dynamics and tunnelling in catalysing hydride transfer: Studies of distal mutants of dihydrofolate reductase. *Philos. Trans. R. Soc. Lond. B Biol. Sci.* **361**, 1307–1315 (2006).
16. M. J. Reddish *et al*., Direct evidence of catalytic heterogeneity in lactate dehydrogenase by temperature jump infrared spectroscopy. *J. Phys. Chem. B* **118**, 10854–10862 (2014).
17. M. D. Blankschien *et al*., Light-triggered biocatalysis using thermophilic enzyme-gold nanoparticle complexes. *ACS Nano* **7**, 654–663 (2013).
18. M. Schade, A. Moretto, P. M. Donaldson, C. Toniolo, P. Hamm, Vibrational energy transport through a capping layer of appropriately designed peptide helices over gold nanoparticles. *Nano Lett.* **10**, 3057–3061 (2010).
19. S. Hassan, M. Schade, C. P. Shaw, R. Lévy, P. Hamm, Response of villin headpiece-capped gold nanoparticles to ultrafast laser heating. *J. Phys. Chem. B* **118**, 7954–7962 (2014).
20. J. R. Adleman, D. A. Boyd, D. G. Goodwin, D. Psaltis, Heterogenous catalysis mediated by plasmon heating. *Nano Lett.* **9**, 4417–4423 (2009).
21. A. O. Govorov, H. H. Richardson, Generating heat with metal nanoparticles. *Nano Today* **2**, 30–38 (2007).
22. S. Maity, L. N. Downen, J. R. Bochinski, L. I. Clarke, Embedded metal nanoparticles as localized heat sources: An alternative processing approach for complex polymeric materials. *Polymer (Guildf.)* **52**, 1674–1685 (2011).
23. J. A. Webb, R. Bardhan, Emerging advances in nanomedicine with engineered gold nanostructures. *Nanoscale* **6**, 2502–2530 (2014).
24. G. Bhabha *et al*., A dynamic knockout reveals that conformational fluctuations influence the chemical step of enzyme catalysis. *Science* **332**, 234–238 (2011).
25. E. J. Loveridge, E. M. Behiry, J. Guo, R. K. Allemann, Evidence that a 'dynamic knockout' in Escherichia coli dihydrofolate reductase does not affect the chemical step of catalysis. *Nat. Chem.* **4**, 292–297 (2012).
26. A. J. Adamczyk, J. Cao, S. C. L. Kamerlin, A. Warshel, Catalysis by dihydrofolate reductase and other enzymes arises from electrostatic preorganization, not conformational motions. *Proc. Natl. Acad. Sci. U.S.A.* **108**, 14115–14120 (2011).
27. C. A. Fierke, K. A. Johnson, S. J. Benkovic, Construction and evaluation of the kinetic scheme associated with dihydrofolate reductase from Escherichia coli. *Biochemistry* **26**, 4085–4092 (1987).
28. P. K. Agarwal, S. R. Billeter, P. T. R. Rajagopalan, S. J. Benkovic, S. Hammes-Schiffer, Network of coupled promoting motions in enzyme catalysis. *Proc. Natl. Acad. Sci. U.S.A.* **99**, 2794–2799 (2002).
29. P. Singh, K. Francis, A. Kohen, Network of remote and local protein dynamics in dihydrofolate reductase catalysis. *ACS Catal.* **5**, 3067–3073 (2015).
30. P. Singh, A. Sen, K. Francis, A. Kohen, Extension and limits of the network of coupled motions correlated to hydride transfer in dihydrofolate reductase. *J. Am. Chem. Soc.* **136**, 2575–2582 (2014).
31. P. K. Agarwal, Role of protein dynamics in reaction rate enhancement by enzymes. *J. Am. Chem. Soc.* **127**, 15248–15256 (2005).
32. F. Liu *et al*., Modulating the activity of protein conjugated to gold nanoparticles by site-directed orientation and surface density of bound protein. *ACS Appl. Mater. Interfaces* **7**, 3717–3724 (2015).
33. L. Shen *et al*., Surface orientation control of site-specifically immobilized nitroreductase (NfsB). *Langmuir* **30**, 5930–5938 (2014).
34. J. P. Lata *et al*., Effects of nanoparticle size on multilayer formation and kinetics of tethered enzymes. *Bioconjug. Chem.* **26**, 1931–1938 (2015).
35. O. Vilanova *et al*., Understanding the kinetics of protein-nanoparticle corona formation. *ACS Nano* **10**, 10842–10850 (2016).
36. W. O. Wray, T. Aida, R. B. Dyer, Photoacoustic cavitation and heat transfer effects in the laser-induced temperature jump in water. *Appl. Phys. B* **74**, 57–66 (2002).
37. L. Swint-Kruse, H. F. Fisher, Enzymatic reaction sequences as coupled multiple traces on a multidimensional landscape. *Trends Biochem. Sci.* **33**, 104–112 (2008).
38. D. D. Boehr, D. McElheny, H. J. Dyson, P. E. Wright, The dynamic energy landscape of dihydrofolate reductase catalysis. *Science* **313**, 1638–1642 (2006).
39. N. S. Galenkamp, A. Biesemans, G. Maglia, Directional conformer exchange in dihydrofolate reductase revealed by single-molecule nanopore recordings. *Nat. Chem.* **12**, 481–488 (2020).
40. M. R. Sawaya, J. Kraut, Loop and subdomain movements in the mechanism of Escherichia coli dihydrofolate reductase: Crystallographic evidence. *Biochemistry* **36**, 586–603 (1997).
41. J. T. Chen, K. Taira, C. P. D. Tu, S. J. Benkovic, Probing the functional role of phenylalanine-31 of Escherichia coli dihydrofolate reductase by site-directed mutagenesis. *Biochemistry* **26**, 4093–4100 (1987).
42. J. R. Hill *et al*., Vibrational dynamics of carbon monoxide at the active sites of mutant heme proteins. *J. Phys. Chem.* **100**, 12100–12107 (1996).
43. H. Fujisaki, J. E. Straub, Vibrational energy relaxation in proteins. *Proc. Natl. Acad. Sci. U.S.A.* **102**, 6726–6731 (2005).
44. D. M. Leitner, Energy flow in proteins. *Annu. Rev. Phys. Chem.* **59**, 233–259 (2008).
45. A. Xie, A. F. van der Meer, R. H. Austin, Excited-state lifetimes of far-infrared collective modes in proteins. *Phys. Rev. Lett.* **88**, 018102 (2002).
46. E. Z. Eisenmesser *et al*., Intrinsic dynamics of an enzyme underlies catalysis. *Nature* **438**, 117–121 (2005).
47. F. A. S. Konuklar, V. Aviyente, T. Haliloğlu, Coupling of structural fluctuations to deamidation reaction in triosephosphate isomerase by Gaussian network model. *Proteins* **62**, 715–727 (2006).
48. V. C. Nashine, S. Hammes-Schiffer, S. J. Benkovic, Coupled motions in enzyme catalysis. *Curr. Opin. Chem. Biol.* **14**, 644–651 (2010).
49. R. L. Blakley, Crystalline dihydropteroylglutamic acid. *Nature* **188**, 231–232 (1960).
50. H. D. Hill, C. A. Mirkin, The bio-barcode assay for the detection of protein and nucleic acid targets using DTT-induced ligand exchange. *Nat. Protoc.* **1**, 324–336 (2006).
51. G. Li, D. Magana, R. B. Dyer, Photoinduced electron transfer in folic acid investigated by ultrafast infrared spectroscopy. *J. Phys. Chem. B* **116**, 3467–3475 (2012).
52. G. Li, D. Magana, R. B. Dyer, Direct observation and control of ultrafast photoinduced twisted intramolecular charge transfer (TICT) in triphenyl-methane dyes. *J. Phys. Chem. B* **116**, 12590–12596 (2012).
53. G. Li, D. Magana, R. B. Dyer, Anisotropic energy flow and allosteric ligand binding in albumin. *Nat. Comm.* **5**, 3100 (2014).
54. R. Kozlowski, A. Ragupathi, R. B. Dyer, Characterizing the surface coverage of protein-gold nanoparticle bioconjugates. *Bioconjug. Chem.* **29**, 2691–2700 (2018).